JOURNAL OF PROPULSION AND POWER
Vol. 9, No. 2, March–April 1993

New Two-Grid Acceleration Method for Unsteady Navier-Stokes Calculations

L. He*
Cambridge University, Cambridge, England, United Kingdom

A quasi-three-dimensional time-marching Navier-Stokes method for calculating unsteady viscous flows in turbomachines is presented. A major feature of the present work is that the time-step limitation in the Navier-Stokes solutions suffered by all explicit time-marching methods is effectively relaxed by using a time-consistent two-grid method. The spatial accuracy is subject to the basic fine mesh, while the coarse mesh, on which the temporal accuracy is guaranteed, is locally applied to the near wall and wake regions to increase the allowable time-step length. The loss of the time accuracy on the basic fine mesh can be easily controlled by choosing a suitable grid size of the coarse mesh according to the wavelength of physical unsteadiness to be dealt with. This two-grid method has been compared with the implicit residual-averaging method and the direct time-marching method for a transonic oscillating cascade flow. Numerical examples for a low-speed oscillating airfoil flow at a dynamic stall condition and a transonic airfoil flow with a self-excited shock oscillation are also presented, in which an increase in the time-step length by a factor of 20 has been achieved.

Nomenclature

C = length of blade chord
C_{p1} = unsteady pressure coefficient
$\mathbf{ds}$ = differential length element with unit outward-pointing normal vector
e = internal energy
f = frequency
K = reduced frequency, $(\omega c/u_\infty)$
k = coefficient of heat conductivity
$\mathbf{n}_x$ = the unit vectors in x direction
Pr = Prandtl number
P_0 = inlet stagnation pressure
P_2 = exit static pressure
p = static pressure
R = gas constant
S = entropy
T = temperature
t = time
U = primitive flow variable
u = velocity in x direction
u_∞ = inlet velocity
v = velocity in y direction
x = axial coordinate
y = pitchwise coordinate
ΔA = area of computational cell
$(\partial x/\partial t)_b$ = moving mesh grid velocity in x direction
μ = laminar viscosity coefficient
μ_T = turbulent viscosity coefficient
ρ = density
τ_w = wall shear stress
ω = angular frequency

Subscripts
c = coarse mesh
f = fine mesh
i = index of mesh point in y direction

Superscript
n = index of time step

Received May 11, 1992; revision received Oct. 2, 1992; accepted for publication Oct. 17, 1992.

*Rolls Royce Senior Research Fellow in Aero-Engineering, Whittle Laboratory/Girton College.

Introduction

UNDERSTANDING and prediction of unsteady viscous flow effect is of great interest in turbomachinery design and analysis. Numerical solution methods for unsteady viscous flows are currently under active development. Efficient methods of coupling an inviscid Euler solver with an integral boundary-layer solution can be used to predict unsteady viscous blockage effects at attached and slightly separated flow conditions (e.g., Refs. 1 and 2). But for highly viscous-dominated flow phenomena where massive flow separation exists (e.g., rotating stall and stall flutter), the Navier-Stokes solutions are required.

The Reynolds-averaged Navier-Stokes solvers are widely used for prediction and analysis of steady turbomachinery flows, though their accuracy is limited by the turbulence closure model. Resolution of thin-viscous layers needs a large number of mesh points. This itself requires more computing resources. Moreover, for an explicit time-marching method, the time-step length is limited by the smallest spatial mesh size, and therefore, the corresponding CPU time for an unsteady flow solution in which a uniform time step must be used would be greatly increased. One can relax the time-step limitation by adopting an implicit scheme. But extra computing effort must be involved in matrix inversion. The coding for an implicit method is also more complicated than that for an explicit one.

Recently, several authors have applied the explicit time-marching method to calculations of unsteady viscous flows in turbomachinery.[3,4] The only temporal convergence acceleration method used in these calculations is the implicit residual averaging which has been widely adopted for steady flow calculations (e.g., Ref. 5). Although in theory, the length of time step should be unlimited if the implicit residual-averaging technique is used, in practice, however, the best convergence is usually achieved with an increase of the time step by a factor of 3–5, compared to a direct explicit scheme. It is noted that the basic idea of the residual-averaging method is to propagate error waves as quickly as possible, which is highly desirable if a steady-state solution is pursued. Unlike the conventional implicit solution methods, the discretized formulation of the implicit residual averaging is, however, completely decoupled from the basic flow governing equations. Therefore, a gain in a larger time step is always associated with a loss in a temporal accuracy. The point is, that the scale on which the temporal accuracy is lost should be clearly measured and controlled against the physical wavelength of the

problems to be modeled. But there seems to be no such a measure in the conventional residual-averaging method.

In this article, an alternative temporal acceleration method based on the concept of the multigrid method (e.g., Ref. 5) is proposed.

Governing Equation, Discretization, and Boundary Condition

The basic methodology is an extension of the method adopted in the author's quasi-three-dimensional inviscid Euler solver for unsteady flows around oscillating blades.[6] The present description will be emphasized on the treatment of the viscous terms.

The integral form of the two-dimensional unsteady Navier-Stokes equations over a moving finite area ΔA is

$$\frac{\partial}{\partial t}\iint_{\Delta A} U\,dx\,dy + \oint_S \left\{\left[F - U\left(\frac{\partial x}{\partial t}\right)_b\right]\boldsymbol{n}_x + \left[G - U\left(\frac{\partial y}{\partial t}\right)_b\right]\boldsymbol{n}_y\right\}\cdot d\boldsymbol{s} = S_v \tag{1}$$

where

$$U = \begin{bmatrix}\rho\\ \rho u\\ \rho v\\ \rho e\end{bmatrix} \quad F = \begin{bmatrix}\rho u\\ \rho uu + p\\ \rho uv\\ (\rho e + p)u\end{bmatrix} \quad G = \begin{bmatrix}\rho v\\ \rho uv\\ \rho vv + p\\ (\rho e + p)v\end{bmatrix}$$

The viscous source term S_v can be modeled at different levels of simplification. In the present work the original form of the full Navier-Stokes equations is adopted

$$S_v = \oint_S [(V_x\boldsymbol{n}_x + V_y\boldsymbol{n}_y]\cdot d\boldsymbol{s} \tag{2}$$

where

$$V_x = \begin{bmatrix}0\\ \tau_{xx}\\ \tau_{xy}\\ -q_x + u\tau_{xx} + v\tau_{xy}\end{bmatrix} \quad V_y = \begin{bmatrix}0\\ \tau_{xy}\\ \tau_{yy}\\ -q_y + u\tau_{xy} + v\tau_{yy}\end{bmatrix}$$

$$\tau_{xy} = \frac{2}{3}\mu\left(2\frac{\partial u}{\partial x} - \frac{\partial v}{\partial y}\right), \quad \tau_{yy} = \frac{2}{3}\mu\left(2\frac{\partial v}{\partial y} - \frac{\partial u}{\partial x}\right)$$

$$\tau_{xy} = \mu\left(\frac{\partial u}{\partial y} + \frac{\partial v}{\partial x}\right), \quad q_x = -k\frac{\partial T}{\partial x}, \quad q_y = -k\frac{\partial T}{\partial y}$$

The coefficient μ is obtained from Sutherland's law with a reference viscosity coefficient being calculated from a fixed Reynolds number at the inlet flow condition. The coefficient k is connected with the viscosity coefficient for Pr by

$$Pr = (C_p\mu/k)$$

For laminar flows, the above set of equations together with the equation of state is readily solvable. For turbulent flows, the equations in the widely used Reynolds-averaged form need a turbulence model to close extra stress and heat flux terms. In the current work, the standard algebraic model of Baldwin and Lomax[7] is adopted, from which μ_T is obtained, based on the local parameters. The effective viscosity coefficient $\mu + \mu_T$, and the effective heat conductivity coefficient $C_p\mu/Pr + C_p\mu_T/Pr_T$ will be used in the calculation. The turbulent Pr_T is taken to be 0.9.

By using the 4-stage Runge-Kutta time-wise integration scheme,[5] the discretized form of Eq. (1) becomes

$$U^{n+1/4} = U^n\frac{\Delta A^n}{\Delta A^{n+1/4}} - \frac{1}{4}\frac{\Delta t}{\Delta A^{n+1/4}}(R_i^n - R_v^n - D^n) \tag{3a}$$

$$U^{n+1/3} = U^n\frac{\Delta A^n}{\Delta A^{n+1/3}} - \frac{1}{3}\frac{\Delta t}{\Delta A^{n+1/3}}(R_i^{n+1/3} - R_v^n - D^n) \tag{3b}$$

$$U^{n+1/2} = U^n\frac{\Delta A^n}{\Delta A^{n+1/2}} - \frac{1}{2}\frac{\Delta t}{\Delta A^{n+1/2}}(R_i^{n+1/2} - R_v^n - D^n) \tag{3c}$$

$$U^{n+1} = U^n\frac{\Delta A^n}{\Delta A^{n+1}} - \frac{\Delta t}{\Delta A^{n+1}}(R_i^{n+1} - R_v^n - D^n) \tag{3d}$$

where

$$R_i = -\sum\left\{\left[F - U\left(\frac{\partial x}{\partial t}\right)_b\right]\Delta y + \left[G - U\left(\frac{\partial y}{\partial t}\right)_b\right]\Delta x\right\}$$

$$R_v = \sum(V_x\Delta y + V_y\Delta x)$$

The summation is taken along the area boundary. The numerical damping term D^n is treated in the same way as in the previous Euler solution.[6] The second-order and fourth-order adaptive smoothing[5] is used in the streamwise direction. In the pitchwise direction, only the second-order smoothing[8] is used. This is because some numerical difficulty was found in implementing the fourth-order smoothing in the pitchwise direction at the blade wall boundaries.[6] Similar to the numerical damping term, the viscous fluxes are only updated at the first stage, which reduces the corresponding viscous part to first-order time accuracy.

The fluxes across each boundary surface of the finite volume are evaluated using flow variables stored at the corners of each cell (i.e., A, B, C, D in Fig. 1). This can be easily carried out for the convective and pressure fluxes. For the viscous fluxes V_x, V_y, the spatial derivatives of flow variables must first be evaluated. Following a method adopted by Liu,[9] an auxiliary cell (a-b-c-d, Fig. 1) around each corner of the original cell is introduced. Similar to the discretization for the governing equations, the spatial derivatives of any flow variable f at the mesh point A can be approximated based on the Gauss theorem by

$$\left(\frac{\partial f}{\partial x}\right)_A = \frac{1}{\Delta A_{abcd}}\sum f\Delta y$$

$$\left(\frac{\partial f}{\partial y}\right)_A = \frac{1}{\Delta A_{abcd}}\sum f\Delta x$$

As far as the boundary conditions are concerned, a major difference between the present solution and the previous Euler solver[6] is in the solid wall condition treatment. Two different conditions have been used. The first one is the nonslip wall condition, in which the velocities are set equal to zero on the wall, and the wall shear stress is evaluated according

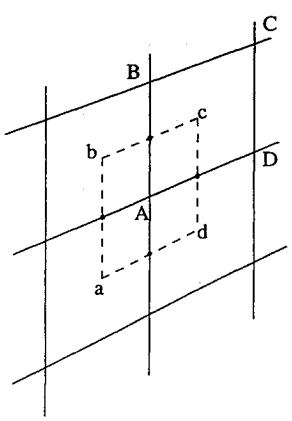

Fig. 1 Finite computational cells.

to the local derivatives. The second method is to set the wall shear stress and allow the velocities to slip. In most cases, the wall shear stress for turbulent flows can be well-described by the log-law. An approximate form of the log-law[10] is used in the present calculations

$$\frac{\tau_w}{0.5\rho_s u_s^2} = -0.001767 + \frac{0.03177}{\ell n(R_e)} + \frac{0.25614}{[\ell n(R_e)]^2}$$

u_s and ρ_s are velocity and density at mesh points one grid spacing (normal distance Δy_n) away from the wall and $R_e = \rho u_s \Delta y_n/\mu$. For laminar flows, the wall shear stress is simply evaluated by $\tau_w = \mu(u_s/\Delta y_n)$. The slip wall condition needs fewer mesh points in the near wall region than the nonslip wall condition, and is used in all the numerical examples presented later, unless otherwise stated.

Two-Grid Time-Marching Method

In a typical H mesh arrangement for unsteady viscous flow calculations, uniformly spaced mesh points in the streamwise direction are usually preferred, because unsteady perturbations of interest (e.g., incoming wakes and incoming/outgoing pressure waves) would have high gradients in any part of the flow domain. In the pitchwise direction, the mesh spacing in the mainly inviscid part of the flowfield can be comparable to that in the streamwise direction, but highly refined mesh points have to be placed in the near wall and wake regions to resolve thin viscous layers. The time step is limited by the smallest mesh size, which is usually the pitchwise length of the mesh cell adjacent to the wall. The present effort is aimed at relaxing the time-step limitation so that a usable time step for an unsteady flow solution would only be subject to the streamwise mesh size (or the pitchwise mesh size in the mainly inviscid part).

Consider that we have two meshes for the time-marching solution. The first mesh is the basic fine mesh on which the flow variables are stored and the fluxes are evaluated. The second mesh is a coarse mesh on which each mesh cell contains several pitchwise cells of the fine mesh. Let us denote the area of a cell on the fine mesh as ΔA_f, and the area of a cell on the coarse as ΔA_c. An example of the two-grid arrangement is given in Fig. 2, in which the first big cell with area ΔA_{c1} contains three small cells with area ΔA_{f1}, ΔA_{f2}, ΔA_{f3}, and the second big cell with area ΔA_{c2} contains two small ones with area ΔA_{f4}, ΔA_{f5}.

For simplicity, we now consider only one-stage temporal integration over a fixed computational cell. If evaluated on a cell of the fine mesh as in a direct time-marching solution, the temporal change of flow variables is

$$(U^{n+1} - U^n)_f = (\Delta t_f/\Delta A_f)R_f \tag{4}$$

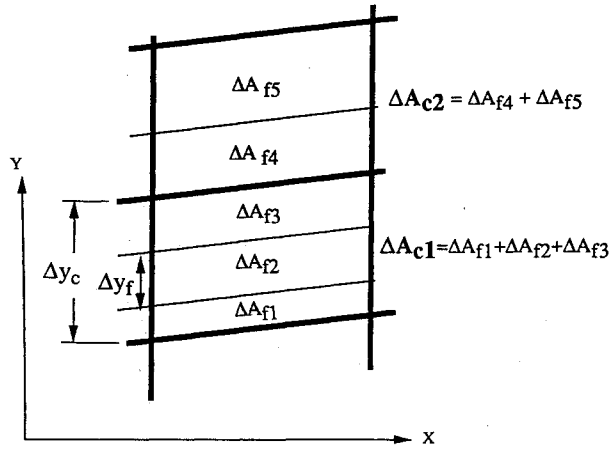

Fig. 2 Two-grid mesh arrangement.

where $R_f = \Sigma[(V_x - F)\Delta y + (V_y - G)\Delta x]_f$. The summation is taken along the boundary of the small cell on the fine mesh with area ΔA_f. While if the temporal change is evaluated on a big cell of the coarse mesh with area ΔA_c, which contains ΔA_f, we have

$$(U^{n+1} - U^n)_c = (\Delta t_c/\Delta A_c)R_c \tag{5}$$

where $R_c = \Sigma[(V_x - F)\Delta y + (V_y - G)\Delta x]_c$. The summation is taken along the boundary of the big cell on the coarse mesh.

The time step Δt_c is limited by the mesh size of the coarse mesh, and therefore, can be much larger than Δt_f. Suppose we want to run an unsteady solution with a uniform time step Δt, which on the fine mesh gives a Courant number CFL, much larger than CFL_0, the one dictated by the numerical stability. The idea is that the temporal integration for a given mesh point should be formulated in such a way as if the solution were time-marched first on the fine mesh up to its stability limit Δt_f, and then on the coarse mesh using Δt_c to make up the desired time step Δt. Thus

$$(U^{n+1} - U^n) = (U^{n+1} - U^n)_f + (U^{n+1} - U^n)_c$$
$$= (\Delta t_f/\Delta A_f)R_f + (\Delta t_c/\Delta A_c)R_c$$

The time-step length on the fine mesh Δt_f is limited by the numerical stability

$$\Delta t_f = \Delta t(\text{CFL}_0/\text{CFL})$$

In order to match the given uniform time-step length Δt after each time step, the time-step length on the coarse mesh Δt_c must be determined for the time consistence

$$\Delta t_c = \Delta t - \Delta t_f = [1 - (\text{CFL}_0/\text{CFL})]\Delta t$$

Therefore, we have

$$(U^{n+1} - U^n) = \frac{R_f}{\Delta A_f}\frac{\text{CFL}_0}{\text{CFL}}\Delta t + \frac{R_c}{\Delta A_c}\left(1 - \frac{\text{CFL}_0}{\text{CFL}}\right)\Delta t \tag{6}$$

In practice, the ratio of the CFL numbers is approximated by the ratio between the pitchwise grid size of the local fine mesh Δy_f, and that in the mainly inviscid part of the flowfield, Δy_{CFL} which limits Δt. And the pitchwise mesh size of the coarse mesh Δy_c should be chosen to be as close to Δy_{CFL} as possible.

The implementation of this two-grid method is very simple because of conservation relations for both areas and fluxes. First, the net fluxes for small cells on the fine mesh are evaluated. The net fluxes for a big cell on the coarse mesh can be directly obtained by a simple summation

$$R_c = \sum_1^{N_{\text{cell}}} R_f$$

N_{cell} is the number of small cells contained in the big cell. Then the temporal change for each small cell can be evaluated by using Eq. (6). In the present calculations, Eq. (6) is applied at each stage of the four-stage Runge-Kutta integration.

For a steady flow solution, this two-grid scheme is equivalent to a direct solution on the fine mesh, because the residual, which drives the solution, is formed based on the net fluxes on the fine mesh. For an unsteady flow solution, the time-wise accuracy on the fine mesh is certainly no longer guaranteed. The loss in the temporal accuracy depends on the local ratio between fine and coarse mesh sizes. In the mainly inviscid flow region far from the wall, the two-grid scheme will reduce to the basic time-marching scheme because $\text{CFL}_0/\text{CFL} = 1$. It should be pointed out that the maximum length scale on which the temporal resolution is lost would

be the mesh spacing length on the coarse mesh. As long as the coarse mesh spacing is taken to be much smaller than the physical wavelength of interest, this loss in time accuracy would be acceptable. Hence, a good balance between efficiency and accuracy can be realized.

Validations

Steady Flat Plate Laminar Boundary Layer

The basic methodology and implementation were first validated by calculating a steady flat plate laminar boundary layer at an incompressible flow condition, for which the analytical similarity solution (the Blasius velocity profile) can be compared. For this laminar boundary layer case, the nonslip wall condition was used. The calculated velocity profile is compared with the Blasius solution, as shown in Fig. 3. Apart from a slightly underpredicted velocity level in the middle part of the profile due to the numerical smoothing, the agreement is excellent.

Transonic Oscillating Cascade Flow

It is considered very useful that the present two-grid method should be compared against the implicit residual-averaging method and the direct time-marching solution at a typical unsteady flow condition of interest. For this reason, the standard implicit residual-averaging method (e.g., Ref. 5) was also implemented. As stated earlier, only the restriction upon the time step by the pitchwise mesh size is of concern. Thus, the residual averaging is only applied in the pitchwise direction. The basic formulation is (e.g., for density)

$$(1 - \varepsilon\delta_{yy})\Delta\rho_i' = \Delta\rho_i \tag{7}$$

where $\Delta\rho_i$ is the nonaveraged temporal change (residual) in a pitchwise cell i, and $\Delta\rho_i'$ is the averaged one. δ_{yy} is the second-difference operator in the pitchwise direction. The smoothing coefficient ε is given by

$$\varepsilon = \tfrac{1}{4}[(\mathrm{CFL}/\mathrm{CFL}_0)^2 - 1]$$

The following discretized form is adopted:

$$-2\varepsilon \frac{\Delta y_{i-1}}{\Delta y_i + \Delta y_{i-1}} \Delta\rho_{i+1}' + (1 + 2\varepsilon)\Delta\rho_i' - 2\varepsilon \frac{\Delta y_i}{\Delta y_i + \Delta y_{i-1}} \Delta\rho_{i-1}' = \Delta\rho_i \tag{8}$$

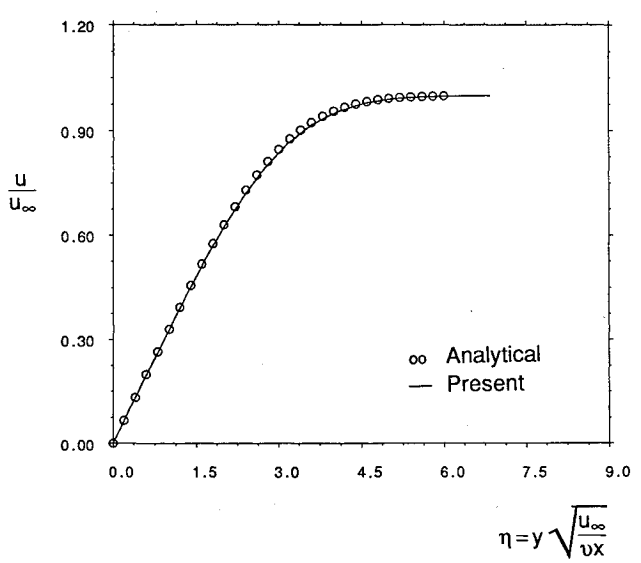

Fig. 3 Blasius similarity velocity profile.

The above implicit residual-averaging method was applied at each stage of the Runge-Kutta integration. It was found by numerical tests that the time step could be increased by a factor of 3–4, compared to the direct solution. Convergence rate would deteriorate rapidly if a larger time step was used.

A transonic oscillating cascade flow was calculated as a test case. The cascade geometry was typical of a transonic fan tip section. The blade was of a biconvex profile with a chord length of 0.1 m, a chord/pitch ratio of 1.3, a maximum thickness of 2%, and a stagger angle of 50 deg. The inlet Mach number was 1.1, Reynolds number was 5×10^5, and the back pressure (P_2/P_0) was 0.64. The flow was assumed to be fully turbulent from the leading edge.

Figure 4 shows the computational mesh (38 × 61). The calculated steady flow Mach number contour is given in Fig.

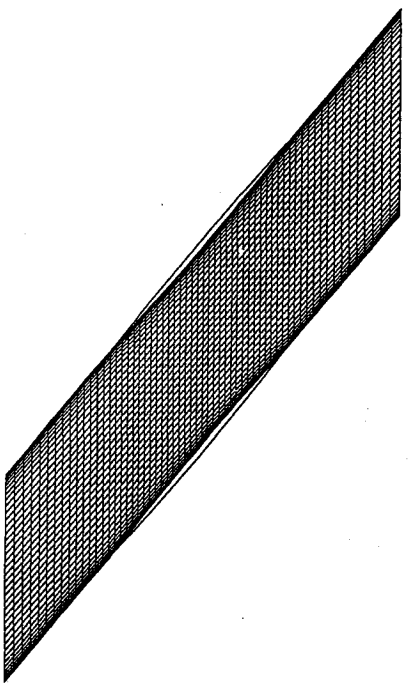

Fig. 4 Computational mesh (38 × 61) for transonic cascade.

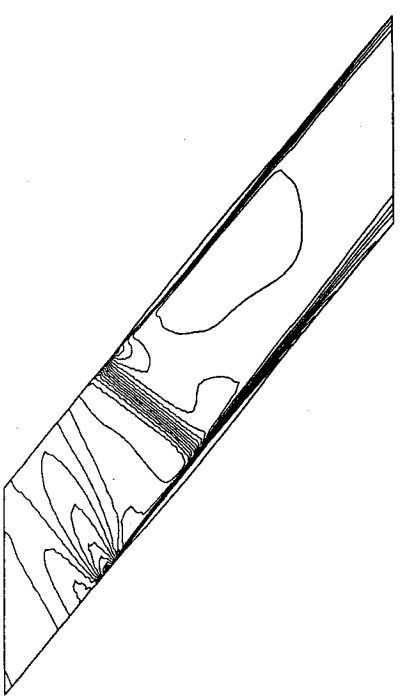

Fig. 5 Steady Mach number contour for transonic cascade.

5, which shows the passage shock with an upstream Mach number about 1.25. The ratio between the pitchwise mesh size in the middle passage and that adjacent to the wall, which limited the time step in the direct time-marching solution, was 3.5/1. In both the two-grid and the residual-averaging solutions, the time step adopted was 3.5 times as large as that used in the direct solution.

The unsteady flow was induced by the cascade oscillating in a torsion mode around the midchord with an amplitude of 0.3 deg, a frequency of 560 Hz (K = 1.1) and an interblade phase angle of 0 deg. The calculated first harmonic unsteady pressure distributions using the two-grid method, the residual-averaging method, and the direct time-marching method, are shown in Fig. 6. It is noticed that the two-grid method and the implicit residual-averaging method gave almost identical results, and both agreed well with the direct solution.

For this case, the extra CPU time required by the two-grid method was 9% compared to the direct solution, while that by the implicit residual averaging was 19%. It must be pointed out, however, that in the two-grid solution, only three big pitchwise cells with the numbers of the small cells in each big cell being 3, 3, 2, were locally used in each of the two near wall regions, because only eight cells in the near wall region were nonuniformly distributed. So the total number of cells involved in the computation for each pitchwise mesh line was 16. While the implicit residual averaging method was applied across the whole passage, i.e., 37 cells were involved in the computation for each pitchwise mesh line. The computing effort in the middle passage region, where the pitchwise mesh points were uniformly distributed, was in fact, wasted. Taking this into account, the actual increases in CPU time for both the two-grid method and the residual-averaging method should be comparable.

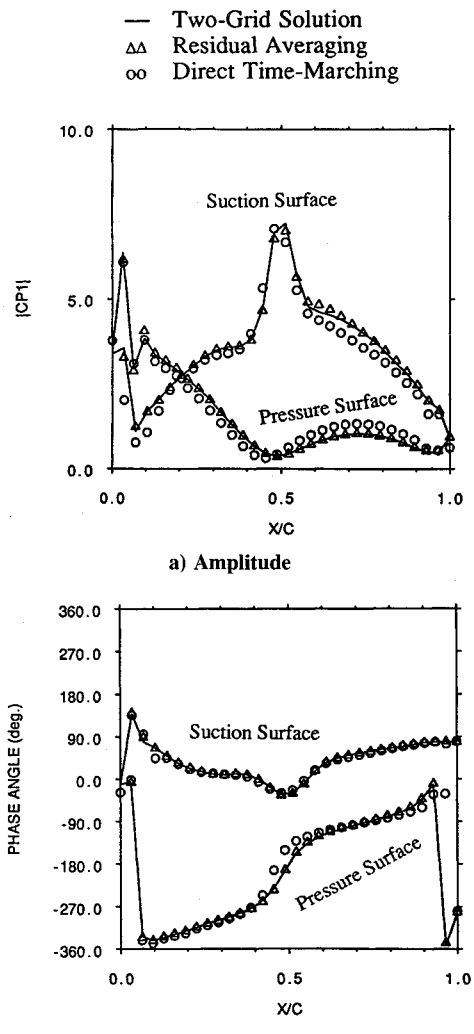

Fig. 6 Unsteady pressure distribution.

Oscillating Airfoil Flow with Dynamic Stall

One of the highly viscous-dominated unsteady flows phenomena around a lifting surface is dynamic stall, which has been well-reported for flows around helicopter airfoils with large oscillation amplitudes (~10 deg). In a recent wind-tunnel experiment with a single airfoil oscillating at a relatively small amplitude (2 deg), a dynamic stall phenomenon with a marked negative aerodynamic damping at a time-mean incidence 10–15 deg was also clearly observed.[11] This experimental case was chosen here to test the ability of the present method to predict the dynamic stall.

The airfoil was the NACA-65 profile with 10% thickness. Although the experiment was conducted at a very low-velocity condition (inlet flow velocity = 25 m/s), the calculation was performed at a Mach number about 0.3, which gave better convergence for the time-marching solution. The two important parameters, the Reynolds number and the reduced frequency of the imposed vibration mode, were kept the same as those in the experiment. The inlet Reynolds number was 2.6×10^5. The time-mean incidence was 10 deg.

Figure 7 shows the computational mesh (100 × 96) with a pitchwise mesh spacing adjacent to the wall being $\frac{1}{20}$ of that in the middle. The corresponding time step used in the present two-grid calculation was about 15 times as large as that for a direct time-marching method. According to the experimental observation, the suction surface was assumed to be turbulent from the leading edge, and the pressure surface was assumed to be laminar. In order to take the tunnel wall viscous effect into account, turbulent boundary layers on the upper and lower tunnel walls were introduced in the calculation from the streamwise position of the airfoil leading edge.

The calculation was first performed at the steady flow condition with the airfoil being stationary. However, it was found

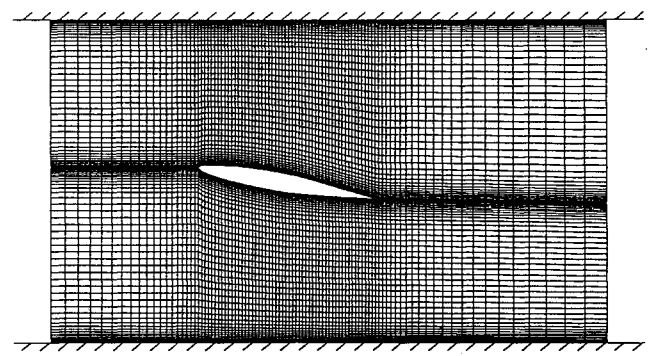

Fig. 7 Computational mesh (100 × 96) for NACA-65 airfoil.

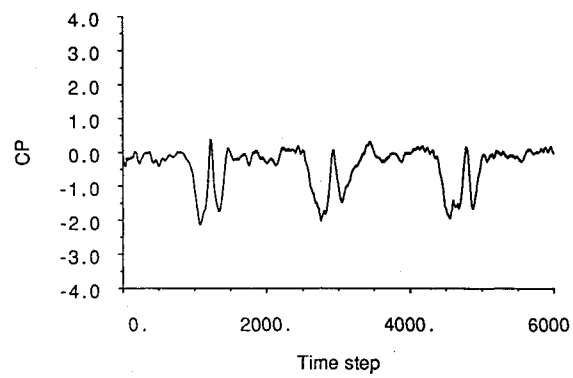

Fig. 8 Time-history of static pressure (90% chord of NACA-65 airfoil under steady conditions).

that a steady flow solution could not be obtained. The suction surface static pressure at the location of 90% chord is plotted in Fig. 8 against the number of time steps with the flowfield starting with a one-dimensional initial guess. This static pressure trace indicates a natural (self-excited) periodic vortex shedding with a reduced frequency about 0.54. However, no clear evidence for the natural vortex shedding at the same scale could be found in the experimental data.

A calculation was then carried out with the same imposed airfoil vibration mode as in the experiment. The airfoil was set to oscillate in torsion around its axis at 42% chord, with a reduced frequency of 0.67. The flow angle, defined as the angle between the chord line and the inlet flow direction changed in the form of

$$\alpha = 10 \text{ deg} + 2 \text{ deg} \sin \omega t$$

The calculated flowfield became very periodic with the frequency of the imposed vibration mode after four periods. This implies that the previous natural (self-excited) vortex shedding mode was now locked to the imposed vibration mode. Figure 9 shows entropy contours at different instants in one period of the airfoil oscillation. Because the entropy is a convective property, the contour lines closely follow the flow

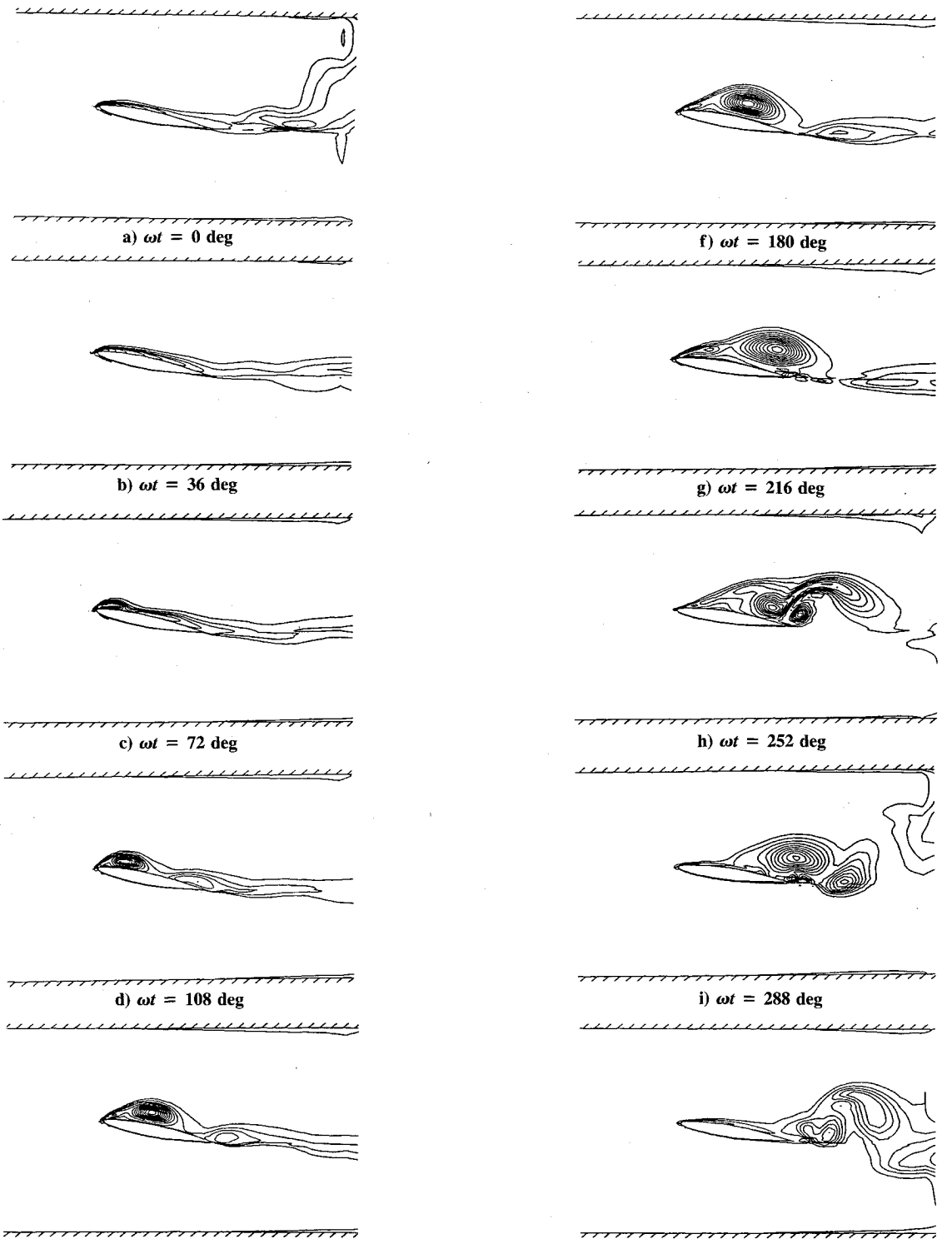

Fig. 9 Entropy [exp(S/R)] contours (interval = 0.015).

particles and give a good indication of vortex movements. As we can see, a leading-edge separation is noticeably enhanced at ωt = 36 deg. A marked leading-edge vortex is formed and transported downstream to the trailing edge between ωt = 72 deg and ωt = 216 deg. Once the big vortex reaches the trailing edge, it interacts with the wakes at the trailing edge, and as a result, a secondary vortex with opposite vorticity is induced (Fig. 9h). Both the primary and the secondary vortices are finally shed from the trailing edge, and the flow pattern then becomes attached as that at ωt = 0 deg. The calculated dynamic stall process agrees qualitatively with the experimental observation.[11] However, the scale of the primary vortex during its downstream movement was considerably overpredicted. The calculated unsteady pressure amplitude on the suction surface near the trailing edge was at least twice as large as the corresponding measured results. Besides, there was no indication of the secondary vortex in the experimental data.

The reasons for these discrepancies are not very clear. One possible reason is that the turbulence model adopted might not be adequate for the present low-speed flow with massive separation. This aspect concerning the turbulence modeling will be further investigated in the future.

Self-Excited Shock Oscillation

Under certain transonic flow conditions, an interaction between a shock and boundary layer around an airfoil trailing

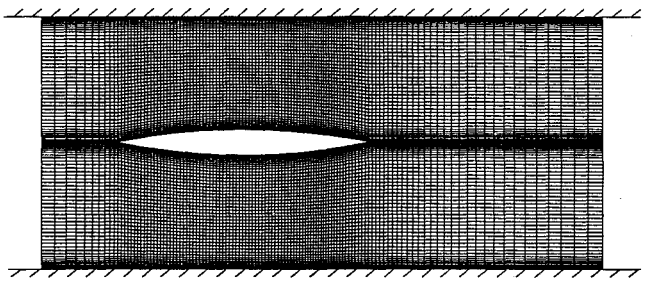

Fig. 10 Computational mesh (120 × 121) for biconvex airfoil.

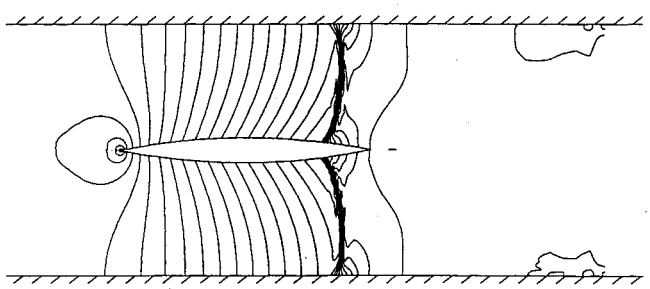

Fig. 11 Static pressure contour (biconvex airfoil).

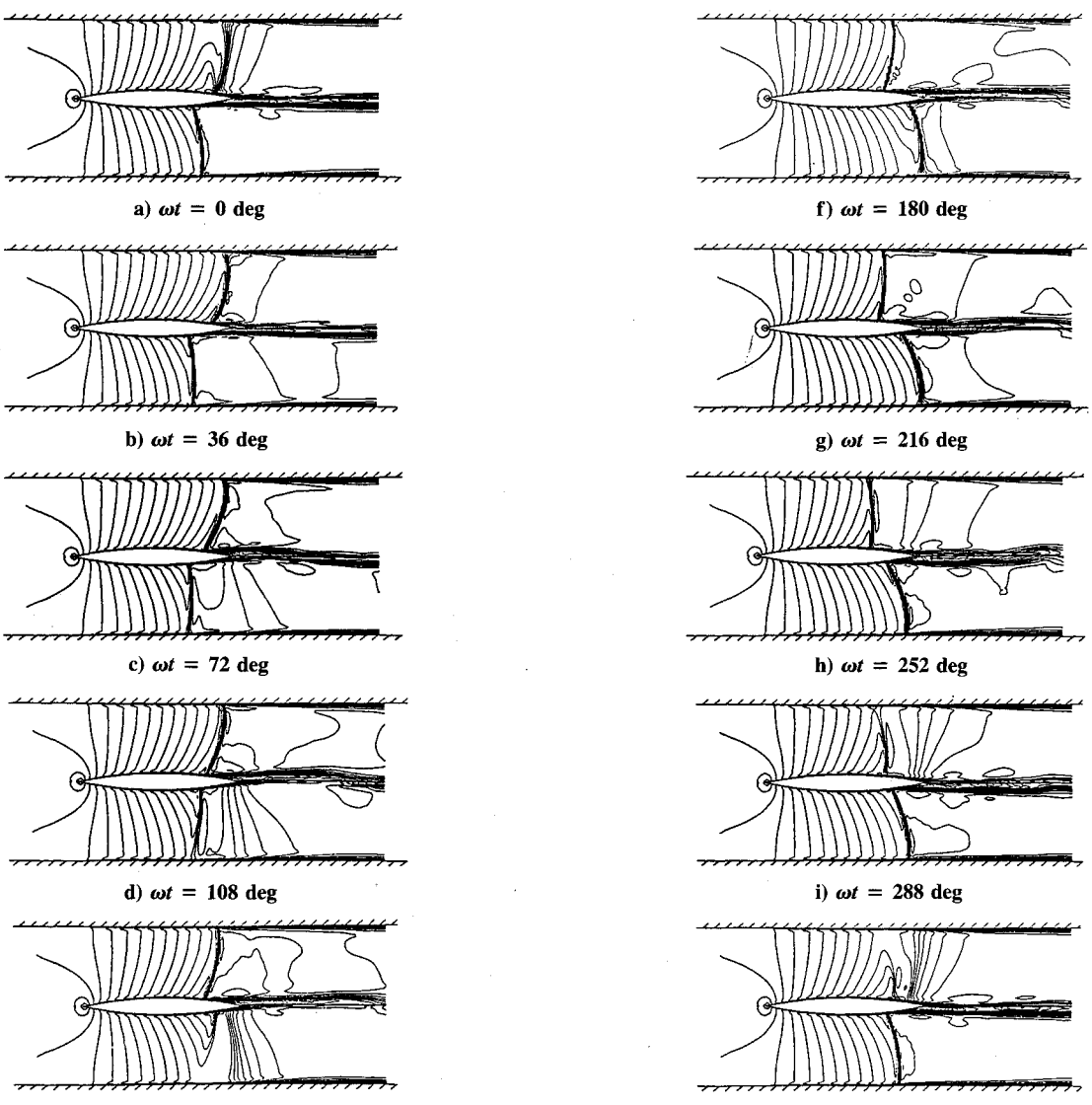

a) ωt = 0 deg

b) ωt = 36 deg

c) ωt = 72 deg

d) ωt = 108 deg

e) ωt = 144 deg

f) ωt = 180 deg

g) ωt = 216 deg

h) ωt = 252 deg

i) ωt = 288 deg

j) ωt = 324 deg

Fig. 12 Mach number contour (interval = 0.05).

edge can generate an unstable aerodynamic mode leading to a periodic self-excited shock oscillation. A detailed experiment for a transonic biconvex airfoil flow was carried out by Yamamoto and Tanida,[12] in which a well-defined self-excited shock oscillation was observed. This unsteady flow case was also chosen here for validating the present method.

The computational mesh (120 × 121) is shown in Fig. 10. The outlet of the computational domain was taken about one chord downstream of the trailing edge. The long duct arrangement downstream of the test section in the experiment was modeled by using the one-dimensional nonreflecting outlet boundary conditions.[15] According to the experiment, the boundary layers on both upper and lower airfoil surfaces were assumed to be turbulent at 10% chord from the leading edge. On the upper and lower tunnel walls, no experimental information about the boundary layers was available. The corresponding tunnel wall viscous effect was approximately taken into account by introducing turbulent boundary layers on both walls at the same streamwise location as the leading edge. It should be mentioned that the maximum pitchwise mesh size ratio was 20, which, by using the present two-grid method, gave a time step 20 times as large as that in a direct time-marching solution. This means that in the present calculation, a net gain in CPU time savings by a factor of 18 was obtained.

The calculation was first performed at a back pressure of $P_2/P_0 = 0.67$ and a Reynolds number of 1×10^6. Figure 11 shows the calculated static pressure contour before the flow becomes unstable, which is roughly of a symmetrical pattern. As the solution was further time marched, the flowfield became apparently asymmetrical, and a well-defined periodicity was established in about 6000 time steps, corresponding to about four periods of the self-excited oscillation. Figure 12 gives Mach number contours at different instants in one oscillation period. The detailed analysis of the corresponding mechanism was given by Yamamoto and Tanida.[13] A space-time contour of static pressure (P/P_0) along a mesh line in the middle of the upper half computational domain is given in Fig. 13a, and the corresponding experimental result ($P_2/P_0 = 0.668$) is given in Fig. 13b. The time scale in terms of ωt in the S-T plot for the calculated result is based on a frequency of 600 Hz, which was the self-excited oscillation frequency measured in the experiment at the same back pressure condition. The calculated mean shock position was further downstream than that shown in the experimental result, which might be mainly due to three-dimensional effects. The comparison between the experiment and the calculation shows a very good agreement in frequency. The agreement in relative phase (the absolute phase is arbitrary) is also fairly good. The amplitude of the shock oscillation, however, was overpredicted by about 60%. A similar phenomenon was also found by Yamamoto and Tanida.[13] The present calculation was then carried out at the back pressure conditions of $P_2/P_0 = 0.66$ and $P_2/P_0 = 0.68$. The calculated self-excited oscillation frequency at $P_2/P_0 = 0.66$ was about 830 Hz, and that at $P_2/P_0 = 0.68$ was about 500 Hz. These calculated frequencies also agree well with the corresponding experimental data.

It should be pointed out that the present calculations agree well with the calculations for this case by Yamamoto and Tanida[13] who used the implicit approximate factorization method[14] and the same Baldwin-Lomax turbulence model as used in the present method.

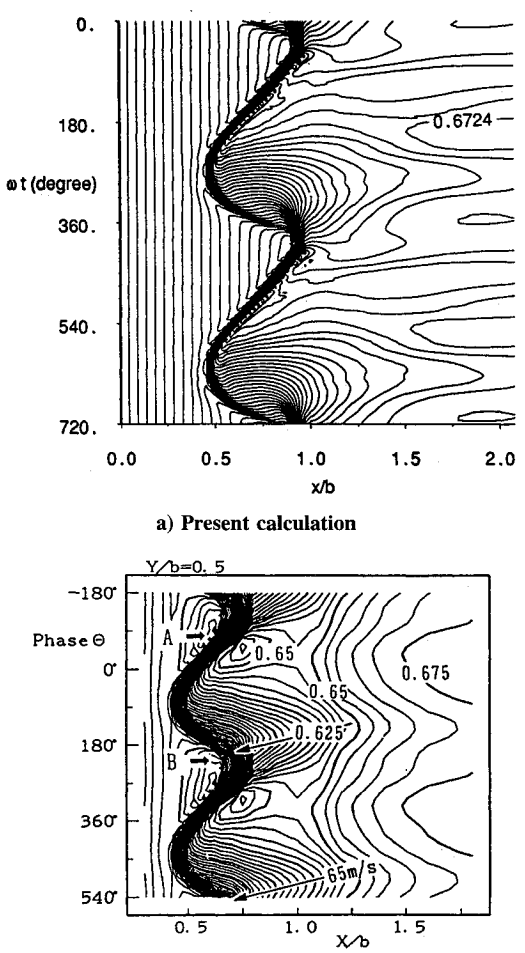

a) Present calculation

b) Measurement

Fig. 13 Space-time contour of static pressure ($b = 0.5c$, $f = 600$ Hz).

Concluding Remarks

An explicit Navier-Stokes time-marching method for calculating unsteady viscous flows in turbomachinery has been developed. The four-stage Runge-Kutta time-wise integration and the cell-vertex finite-volume spatial discretization were adopted. The Baldwin-Lomax algebraic model was used for the turbulence closure.

A major feature in the present work is that the time-step limitation suffered by the explicit methods is very effectively relaxed by using a new two-grid method. In this two-grid method, the spatial resolution is subject to the basic fine mesh. In order to achieve a large usable time step for unsteady viscous flow calculations, a coarse mesh, on which the temporal resolution is maintained, is locally applied to the near wall and wake regions. The most inaccurate temporal resolution occurs on the smallest mesh cell, and the length scale on which the time accuracy would be lost is the mesh size of the coarse mesh. Therefore, by choosing a suitable spacing for the coarse mesh against the physical wavelength of the unsteady flow problems to be modeled, the loss in the time-wise accuracy can be clearly controlled. Compared to the conventional implicit residual-averaging method, the present two-grid method has a more physically sound base and is easier to implement. With a similar amount of extra CPU time to the implicit residual-averaging method, a much larger time step can be used. Therefore, a very good balance between accuracy and efficiency can be achieved for unsteady viscous flow calculations.

Calculated results for a transonic oscillating cascade at a typical frequency of interest are in good agreement with those by using the direct time-marching and the implicit residual averaging. A dynamic stall phenomenon has been predicted for a highly loaded oscillating airfoil in a low-speed wind tunnel, but calculated results only correlate with the corresponding experiment in a qualitative sense. Finally, a calculation has been carried out for a transonic flow around a symmetrical airfoil and the calculated asymmetrical self-excited shock oscillation agree well with the corresponding experimental data. Also, in this case, an increase of the time step by a factor of 20 (a net payoff on CPU savings by a factor

of 18), compared to the direct time-marching solution, has been achieved.

Acknowledgments

The present work has been supported by Rolls-Royce plc. The author is very grateful to John Denton for his help during the course of this study. The author wishes to thank Peter Stow and Arj Suddhoo of Rolls-Royce for their technical support.

References

[1]He, L., and Denton, J. D., "Inviscid-Viscous Coupled Solution for Unsteady Flows Through Oscillating Blades, Part 1. Description of the Method," American Society for Mechanical Engineers Paper 91-GT-125, June 1991; see also *Journal of Turbomachinery* (to be published).

[2]He, L., and Denton, J. D., "Inviscid-Viscous Coupled Solution for Unsteady Flows Through Oscillating Blades, Part 2. Computational Results," American Society for Mechanical Engineers Paper 91-GT-126; see also *Journal of Turbomachinery* (to be published).

[3]Jongenson, P., and Chima, R., "An Unconditionally Stable Runge-Kutta Method for Unsteady Flows," AIAA Paper 89-0205, Jan. 1989.

[4]Rao, K., and Delaney, R., "Investigation of Unsteady Flow Through Transonic Turbine Stage," AIAA Paper 90-2408, July 1990.

[5]Jameson, A., "Numerical Solution of the Euler Solution for Compressible Inviscid Fluids," Princeton Univ., Rept. MAE 1643, Princeton, NJ, Oct. 1983.

[6]He, L., "An Euler Solution for Unsteady Flows Around Oscillating Blades," *Journal of Turbomachinery*, Vol. 112, No. 4, 1990, pp. 714–722.

[7]Baldwin, B. S., and Lomax, H., "Thin Layer Approximation and Algebraic Model for Separated Turbulent Flows," AIAA Paper 78-0257, Jan. 1978.

[8]Denton, J. D., "An Improved Time Marching Method for Turbomachinery Flow Calculations," *Journal of Engineering for Power*, Vol. 105, No. 3, 1983, pp. 514–524.

[9]Liu, F., "Numerical Calculation of Turbomachinery Cascade Flows," Ph.D. Dissertation, Princeton Univ., Dept. of Mechanical and Aerospace Engineering, Princeton, NJ, June 1991.

[10]Denton, J. D., private communication, Cambridge Univ., Cambridge, England, UK, Feb. 1992.

[11]He, L., and Denton, J. D., "An Experiment on Unsteady Flows over an Oscillating Airfoil," American Society for Mechanical Engineers Paper 91-GT-181, June 1991.

[12]Yamamoto, K., and Tanida, Y., "Self-Excited Oscillation of Shock Waves on an Airfoil in Two-Dimensional Transonic Channel Flow," *Proceedings of the 4th Symposium on Unsteady Aerodynamics and Aeroelasticity in Turbomachines and Propellers*, Aachen, Germany, Sept. 1987, pp. 769–783.

[13]Yamamoto, K., and Tanida, Y. "Self-Excited Oscillation of Transonic Flow Around an Airfoil in Two-Dimensional Channel," American Society of Mechanical Engineers Paper 89-GT-58, June 1989.

[14]Beam, R. M., and Warming R. F., "An Implicit Factored Scheme for the Compressible Navier-Stokes Equation," AIAA Paper 77-645, June 1977.

[15]Giles, M. B., "Nonreflecting Boundary Conditions for Euler Equation Calculations," *AIAA Journal*, Vol. 28, No. 12, 1990, pp. 2050–2058.